

## Article

# Mechanical Characterization of the Male Lower Urinary Tract: Comparison among Soft Tissues from the Same Human Case Study

Alice Berardo <sup>1,2,3,†</sup> , Maria Vittoria Mascolini <sup>4,†</sup> , Chiara Giulia Fontanella <sup>2,4,\*</sup> , Martina Contran <sup>5</sup>,  
Martina Todesco <sup>1</sup> , Andrea Porzionato <sup>5,6,7</sup> , Veronica Macchi <sup>5,6,7</sup> , Raffaele De Caro <sup>5,6,7</sup> ,  
Rafael Boscolo-Berto <sup>5,6,7,‡</sup> and Emanuele Luigi Carniel <sup>2,4,‡</sup> 

- <sup>1</sup> Department of Civil, Environmental and Architectural Engineering, University of Padova, 35131 Padova, Italy; alice.berardo@unipd.it (A.B.); martina.todesco@unipd.it (M.T.)
  - <sup>2</sup> Centre for Mechanics of Biological Materials, University of Padova, 35131 Padova, Italy; emanueleluigi.carniel@unipd.it
  - <sup>3</sup> Department of Biomedical Sciences, University of Padova, 35131 Padova, Italy
  - <sup>4</sup> Department of Industrial Engineering, University of Padova, 35131 Padova, Italy; mariavittoria.mascolini@phd.unipd.it
  - <sup>5</sup> Department of Neuroscience, Institute of Human Anatomy, University of Padova, 35121 Padova, Italy; martina.contran@unipd.it (M.C.); andrea.porzionato@unipd.it (A.P.); veronica.macchi@unipd.it (V.M.); raffaele.decaro@unipd.it (R.D.C.); rafael.boscoloberto@unipd.it (R.B.-B.)
  - <sup>6</sup> Veneto Region Reference Centre for the Preservation and Use of Gifted Bodies, Veneto Region, 35100 Padua, Italy
  - <sup>7</sup> National Reference Centre for the Preservation and Use of Gifted Bodies, 35121 Padua, Italy
- \* Correspondence: chiara giulia.fontanella@unipd.it  
† These authors contributed equally to this work.  
‡ These authors are both last authors of the work.



**Citation:** Berardo, A.; Mascolini, M.V.; Fontanella, C.G.; Contran, M.; Todesco, M.; Porzionato, A.; Macchi, V.; De Caro, R.; Boscolo-Berto, R.; Carniel, E.L. Mechanical Characterization of the Male Lower Urinary Tract: Comparison among Soft Tissues from the Same Human Case Study. *Appl. Sci.* **2024**, *14*, 1357. <https://doi.org/10.3390/app14041357>

Academic Editor: Arkady Voloshin

Received: 18 December 2023

Revised: 11 January 2024

Accepted: 26 January 2024

Published: 7 February 2024



**Copyright:** © 2024 by the authors. Licensee MDPI, Basel, Switzerland. This article is an open access article distributed under the terms and conditions of the Creative Commons Attribution (CC BY) license (<https://creativecommons.org/licenses/by/4.0/>).

**Featured Application:** An exhaustive mechanical characterization of the lower urinary tract represents a key point for the development of effective in silico models to provide additional information on dysfunctions and validate innovative devices for the treatment of related pathologies.

**Abstract:** Background: Nowadays, a challenging task concerns the biomechanical study of the human lower urinary tract (LUT) due to the variety of its tissues and the low availability of samples. Methods: This work attempted to further extend the knowledge through a comprehensive mechanical characterization of the male LUT by considering numerous tissues harvested from the same cadaver, including some never studied before. Samples of the bladder, urethra, prostate, Buck's fascia and tunica albuginea related to corpora cavernosa were considered and distinguished according to testing direction, specimen conformation and anatomical region. Uniaxial tensile and indentation tests were performed and ad hoc protocols were developed. Results: The tissues showed a non-linear and viscoelastic response but different mechanical properties due to their specific functionality and microstructural configuration. Tunica albuginea longitudinally displayed the highest stiffness (12.77 MPa), while the prostate transversally had the lowest one (0.66 MPa). The minimum stress relaxation degree (65.74%) was reached by the tunica albuginea and the maximum (88.55%) by the bladder. The prostate elastic modulus was shown to vary according to the presence of pathological changes at the microstructure. Conclusions: This is the first experimental work that considers the mechanical evaluation of the LUT tissues in relation to the same subject, setting the basis for future developments by expanding the sample population and for the development of effective in silico models to improve the solutions for most LUT pathologies.

**Keywords:** lower urinary tract; human soft tissue; urethral tissues; mechanical tests; prostate; bladder; tunica albuginea; Buck's fascia

## 1. Introduction

The human male lower urinary tract (LUT) consists of the bladder and the urethra, which in combination allow the storage and the voiding of urine. The bladder is the distensible and hollow organ acting as the reservoir of urine and in continuous connection to the upper urinary tract through the two ureters and to the urethra through its lowest part, the neck [1]. The urethra is the duct through which the urine passes and it is distinct along its length, from the bladder neck to the external urethral orifice, in five segments (pre-prostatic, prostatic, membranous, bulbar and penile). In males, the LUT is also completed by other tissues, such as the prostate, the Buck's fascia and the tunica albuginea, that are anatomically and functionally related to the main components. The prostate, immediately below the bladder neck, is an inverted pyramid-shaped gland surrounding the urethra in the prostatic region. In the distal region, the urethra passes through the corpus spongiosum, which composes the penis together with the two corpora cavernosa [2]. The Buck's fascia surrounds as a whole the corpus spongiosum and corpora cavernosa, each of which is enveloped by its own layer of tunica albuginea, which is thinner for the corpus spongiosum.

All these LUT components are soft connective tissues characterized by specific microstructural configurations determining their mechanical properties. The mechanical behavior of many human tissues has already been extensively investigated [3], but the research in LUT biomechanics is still at an early stage, mainly due to the heterogeneity of the tissues involved and the difficulty in the availability of samples. To date, few works in literature have analyzed the mechanics of these tissues.

Regarding the urethral tissue, in 2018 Masri et al. [4] mechanically characterized five human urethrae from male cadavers by separating membranous and spongy urethra portions and then testing the samples along the longitudinal and circumferential directions, while in 2020, Cunnane et al. [5] performed mechanical tests on human male urethrae obtained from patients that underwent gender reassignment surgery. The results revealed a nonlinear response with stiffening at higher pressures during both static and dynamic loadings and pronounced viscoelastic behavior with increasing stretch. In addition, Cunnane et al. also performed tensile tests by considering ring portions of the bulbar and penile urethra from the distal and proximal regions [5]. No difference between the directional responses at any stress was observed as well as between regional responses during circumferential or longitudinal extension and in terms of the relaxation or creep parameters defining the response in the two directions.

Lalla et al. [6] investigated the biomechanical properties in a rabbit model to test hypospadias operations by stretching ring specimens until rupture. In the same context of the failure tensile test, in 2021 Cunnane et al. [7] mechanically characterized 18 porcine urethral tissue subjected to different cryopreservation protocols to identify the one that best preserved the native tissue properties. The findings showed that urethral tissue should be stored at  $-20\text{ }^{\circ}\text{C}$ , while the storage at  $-80\text{ }^{\circ}\text{C}$  resulted in significantly altering the mechanical properties, failure mechanics and geometry of the tissue. Finally, Natali et al. [8] selected the equine urethra as a suitable animal model due to the similarity in terms of the lumen, histo-morphometric conformation and functional process of micturition to the human urethra. Tensile, stress-relaxation and inflation tests were performed. A significant difference in terms of stiffness resulted when the longitudinal proximal specimens were compared to all the other samples.

As concerns the mechanical investigation of the bladder tissue, in 2012, Zanetti et al. [9] studied the effect of strain rate, orientation and loading history on the behavior of porcine bladder tissue. In 2015 Natali et al. [10] performed uniaxial cyclic tests on porcine samples at different strain rates (10, 50, 100, 200,  $500\% \text{ s}^{-1}$ ). Transverse specimens showed greater stiffness and influence of the strain rate than those exhibited by apex-to-base ones.

Concerning prostate tissue, most of the biomechanical research has been carried out to study the changes in the mechanical properties of pathological conditions. Krouskop et al. [11] considered 113 specimens from human normal, benign prostatic hyperplasia (BPH) and cancer prostate tissues, which were cut into slab-shaped samples and tested under in-

dentation, revealing that tissue from prostate with BPH resulted significantly softer than normal tissue, while cancers significantly stiffer than normal tissue at both strain ranges. Phipps et al. [12] collected 85 fresh chippings via transurethral resection of the prostate (TURP) from 17 patients with an ad hoc system for mechanical testing through an electromechanical shaker inducing a cyclic compressive load at actuation frequencies between 5 and 50 Hz to derive strong correlations between mechanical properties and morphology of the prostatic tissue, which may allow a more accurate prediction of the response to a given therapy [12]. Other indentation tests were also performed by Ahn et al. [13] and Kim et al. [14], while Ma et al. [15] tested prostate samples, cut parallel and perpendicular to the urethra, through uniaxial load–unload mechanical testing. Both healthy (cadaveric) as well as periurethral tissues obtained from radical prostatectomy were analyzed. These latter reported a wider range of tangent modulus with greater stiffness directly correlated with higher collagen content due to fibrosis and with moderate/severe LUT symptoms.

The mechanical basis of the tunica albuginea was only partially studied in human health conditions [16] or disease [17], and in an animal model [18]. In 1990, Bitsch et al. [16] performed tensile tests up to failure by adopting a tensiometer and exposing the samples to a stepwise increasing pressure. In 2022, Brady et al. [17] designed a testing strategy to characterize the mechanical properties of the tunica albuginea affected by Peyronie’s Disease (PD), a progressive fibrosis that can cause tissue mineralization. Uniaxial tensile tests up to failure showed an altered tissue behavior with mineralization, supported by the literature studies on the atherosclerotic plaque mechanics which found higher moduli [19–21] in calcified plaques compared to healthy tissue.

No published studies investigated the biomechanical behavior of Buck’s fascia or studied the overall mechanical properties of the different LUT tissues from the same subject. This ongoing challenge is attracting considerable interest among the scientific community due to the close relationship between the functionality of LUT constituent tissues and their mechanical performances. Assessing the mechanical response and identifying and validating the constitutive models of the entire LUT are fundamental steps to develop *in silico* models for surgical procedures and prosthesis design in order to propose alternative and innovative solutions for most pathologies, such as urinary incontinence and BPH, that nowadays are not always optimized or effective.

For the first time, this study aimed to simultaneously mechanically characterize the soft tissues composing the entire human male LUT, thanks to the combination of multiple mechanical tests (uniaxial tensile tests up to failure, stress–relaxation tests and indentation tests) on five different tissues, cut along different directions when possible. Bladder, urethra, prostate, Buck’s fascia and tunica albuginea related to corpora cavernosa were obtained from a fresh-frozen 77-year-old male cadaver donor, according to the Body Donation Program of the Institute of Anatomy of the University of Padua [22].

Quantification and evaluation of the mechanical failure and time-dependent properties were performed, analyzing similarities and differences between tissues according to their functionality and in relation to the same subject. In addition, histological analyses were carried out to confirm the obtained results. This work could represent a turning point in advancing the development of effective *in silico* models for studying LUT dysfunctions. It could also contribute to the design of devices for treating LUT pathologies, the creation of reliable tissue response-mimicking phantoms for surgical planning, and advancements in tissue engineering. These applications extend from anatomical surgical reconstruction to addressing functional defects in the LUT.

## 2. Materials and Methods

### 2.1. Tissues Harvesting

In accordance with the Body Donation Program of the Institute of Anatomy of the University of Padua [22], bladder, urethra, prostate, Buck’s fascia and tunica albuginea related to corpora cavernosa were obtained, without apparent anomalies, from a fresh-frozen 77-year-old male cadaver. His clinical records reported a remote TURP without

significant complications or sequelae that could have affected the LUT tissues and functions. The gross in situ dissection and the following microscopic examination of the harvested tissue were consistent with the donor's medical history. The urethra and prostate were acquired entirely as structures, while other tissues were harvested as patches. Tissues were stored at  $-20\text{ }^{\circ}\text{C}$  and thawed before testing.

## 2.2. Sample Preparation

All tissues were accurately prepared for the mechanical testing, according to the typology of the test and the nature and origin of the tissue (Figure 1). To perform the uniaxial tensile tests, rectangular strip or ring samples were used.

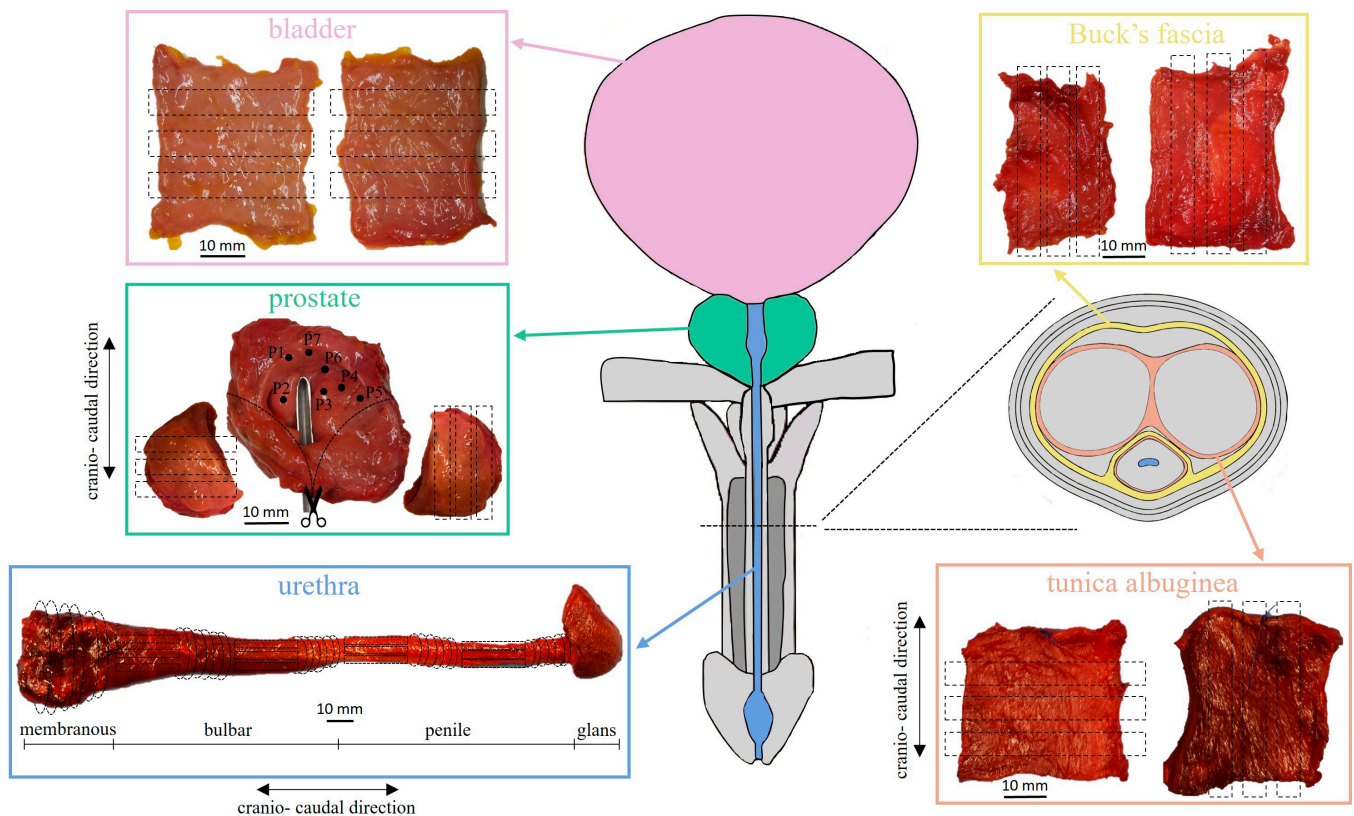


**Figure 1.** Anatomical illustration of the human male LUT and cross-section of the penis showing the relationship between bladder, urethra, prostate, Buck's fascia and tunica albuginea. For each acquired tissue, details for sample preparation are reported.

Bladder patches were cut in rectangular strips amounting to 6 samples (as reported in Table 1) with mean  $\pm$  standard deviation (SD) width of  $4.47 \pm 0.67$  mm and length of  $19.71 \pm 0.73$  mm, as well as for Buck's fascia (width  $2.17 \pm 0.73$  mm, length  $20.00 \pm 0.00$  mm). In these cases, only one cut direction was considered because the specific harvesting site was unknown for the bladder, while no references were found in literature about Buck's fascia biomechanics since it appears a quite new field of research.

Secondly, tunica albuginea of the corpora cavernosa was tested along longitudinal and transversal directions with respect to the urethra, thus 5 rectangular strips (Table 1) were obtained from its native patch (width  $3.44 \pm 0.94$  mm, length  $19.82 \pm 0.60$  mm). The anisotropy was also investigated for the urethra and the prostate, according to the literature [4,5,8,15]. The extracted urethra, from the proximal to the distal end, included the membranous, bulbar and penile portions (Figure 1). For this reason, it was firstly transversally sectioned to distinguish the 3 specific portions. The membranous portion was again transversally cut obtaining 3 rings samples (Table 1) with a mean width of  $4.31 \pm 0.46$  mm. On the other hand, both bulbar and penile portions were transversally

sectioned in the middle to distinguish the distal and the proximal regions. Successively, each region of both urethral portions was transversally dissected obtaining 3 rings with a mean width of  $4.52 \pm 0.71$  mm and a remaining wider ring, which was incised longitudinally and straightened. From this latter, 4 rectangular strips with an average width of  $6.81 \pm 1.47$  mm and length of  $14.53 \pm 8.35$  mm were obtained for each region. In total, 8 longitudinal and 6 transversal samples were gathered for both the bulbar and the penile urethral portions (Table 1).

**Table 1.** For each type of test and kind of tissue, the number of samples is reported together with the directions studied.

Test	Type	Tissue	No. of Samples	Direction	
Uniaxial tensile	Failure	Bladder	6	-	
		Buck's fascia	6	-	
		Prostate	8	Longitudinal (#5) Transversal (#3)	
	Stress–relaxation	Tunica albuginea		5	Longitudinal (#3) Transversal (#2)
			Bladder	6	-
			Tunica albuginea	3	Transversal
			Membranous urethra	3	Transversal
		Bulbar urethra	14	Longitudinal (#8) Transversal (#6)	
			Penile urethra	14	Longitudinal (#8) Transversal (#6)
		Indentation		Prostate	1

The acquired prostate was cut longitudinally in the apex region and the right and left lateral sides were isolated from the central portion. From the right side, 5 rectangular strips were trimmed along the direction longitudinal to the urethra, while 3 analogous samples, from the left side, were obtained along the transversal direction (width  $8.01 \pm 2.83$  mm, length  $16.25 \pm 5.18$  mm). On the remaining prostate part, indentation tests were performed. Both during and after the preparation procedure, a phosphate-buffered saline solution was used to keep all the samples moist so as not to alter their mechanical properties due to non-physiological dehydration.

Moreover, for the strip specimens, a further final step of preparation was performed by using a paper C-shaped support. Each end of the samples was interposed between one extremity of the support and a small paper strip, to which the Velcro was glued. The male sides of the Velcro in addition to a medical-grade cyanoacrylate glue (Glue Loctite 4013 Prism, Hisco, Houston, TX, USA) on their surface were used to fix the ends of the samples, facilitating their positioning within the grips of the mechanical tester and avoiding both the slippage and the misalignment of the specimens. In addition, the so prepared samples were clamped by adequate grips with textured pattern surfaces, and the closure pressure was adjusted to ensure the fixation but, at the same time, the absence of tissue damage. Afterward, the C-shaped support was cut along its length to allow the mechanical test. On the other hand, the ring specimens did not require any additional preparation, they were slid over the top and bottom posts of a T-shaped tensile fixture (post diameter 0.8 mm), specifically developed for the mechanical evaluation of small ring of material [23].

For all samples prepared for tensile tests, the grip-to-grip length and width were defined through the image processing software ImageJ (NIH, Bethesda, MD, USA, version 1.54d, 2020) while the thickness was measured by means of a manual caliper of 0.1 mm resolution at different positions along the length of the sample and the average value was finally considered. Mean  $\pm$  SD values of width, thickness and length of the samples are reported in Table 2 for each tissue studied.

**Table 2.** For each tissue, mean  $\pm$  SD values of width, thickness and length are reported in mm.

Tissue	Specimen	Width (Mean $\pm$ SD)	Thickness (Mean $\pm$ SD)	Length (Mean $\pm$ SD)
Bladder	Strip	4.47 $\pm$ 0.67	2.14 $\pm$ 0.31	19.71 $\pm$ 0.73
Buck's fascia	Strip	2.17 $\pm$ 0.73	0.87 $\pm$ 0.49	20.00 $\pm$ 0.00
Prostate	Strip	8.01 $\pm$ 2.83	1.96 $\pm$ 0.62	16.25 $\pm$ 5.18
Tunica albuginea	Strip	3.44 $\pm$ 0.94	2.38 $\pm$ 0.52	19.82 $\pm$ 0.60
Membranous urethra	Ring	4.31 $\pm$ 0.46	8.63 $\pm$ 2.85	14.34 $\pm$ 4.04
Bulbar urethra	Ring	4.76 $\pm$ 0.19	9.57 $\pm$ 1.56	14.00 $\pm$ 3.79
Penile urethra	Strip	7.12 $\pm$ 1.68	3.79 $\pm$ 0.99	21.45 $\pm$ 1.94
	Ring	4.29 $\pm$ 0.98	8.09 $\pm$ 0.91	13.83 $\pm$ 2.56
	Strip	6.47 $\pm$ 1.20	3.66 $\pm$ 0.51	22.87 $\pm$ 2.47

### 2.3. Experimental Protocols

Tests were performed at room temperature by means of the mechanical tester Biomechanism Mach-1 v500csst (Laval, QC, Canada) equipped with a 3-axis motion controller (resolution of 0.5  $\mu\text{m}$ , max acceleration of 500  $\text{mm/s}^2$ ) and a uniaxial load cell of 250 N (accuracy of 0.0125 N). Experimental protocols for uniaxial tensile tests adopted for each tissue and indentation tests for the prostate tissue are reported below.

#### 2.3.1. Uniaxial Tensile Test

Prior to the tensile tests, all the samples were subjected to a first preconditioning phase through the application of a sinusoidal displacement curve (consisting of 10 cycles), for a total applied strain of 5% and a curve frequency of 1.5 Hz. Then, the issue was allowed to recover during a resting phase of 30 s before starting the effective test.

Uniaxial tensile tests up to failure or stress–relaxation tests were performed. In detail, bladder, Buck's fascia, prostate and tunica albuginea strips were tested up to the failure by applying a progressive strain with a strain rate of 2.5%  $\text{s}^{-1}$  (as shown in Table 3). The tests were stopped when a decreasing force was measured or visible damage to the tissue was observed.

**Table 3.** Experimental protocol adopted according to the different biological tissues.

Test	Tissue	Strain Rate [% $\text{s}^{-1}$ ]	No. of Ramps	Strain Step [%]	Resting Time [s]
Failure	Bladder	2.5	-	-	-
	Buck's fascia	2.5	-	-	-
	Prostate	2.5	-	-	-
	Tunica albuginea	2.5	-	-	-
Stress–relaxation	Bladder	30	5	10	300
	Tunica albuginea	30	4	10	300
	Urethra	30	6	10	400

On the other hand, the stress–relaxation protocol included a defined number of consecutive almost instantaneous (strain rate of 30%  $\text{s}^{-1}$ ) elongations, with each step of 10% strain and held constant for a fixed resting time. In particular, for the bladder 5 strain steps and a relaxation time of 300 s were considered, for the tunica albuginea 4 strain steps and 400 s of relaxation time were considered and for the urethra 6 strain steps and 400 s of relaxation time were considered (Table 3).

#### 2.3.2. Indentation Test

The indentation test was performed only for the prostate, due to the limited sample availability for the other tissues. The central portion of the acquired prostate was placed on a flat base, to which the Velcro was glued to guarantee adherence and attachment to keep the sample fixed during the test. The anterior surface was measured by identifying 7 indentation sites which could represent the peculiarities and variability of the tissue

(Figure 1). The test was carried out by means of a spherical tip indenter (radius  $R$  of 3.18 mm) inducing an increasing indentation depth up to 4 mm at  $0.2 \text{ mm s}^{-1}$ . The indentations started once the load cell found contact with the tissue.

#### 2.4. Histological Evaluations

Among the selected tissues, patch samples of the bladder and tunica albuginea related to corpora cavernosa were harvested with a dimension of  $5 \text{ mm} \times 20 \text{ mm}$ . Moreover, 5 mm thickness transversal sections of the whole prostate and penis were cut to obtain macrosections. All tissues were fixed for one week in formaldehyde 4% *m/v*, buffered according to Lille, pH 6.9 (100496, Sigma Aldrich, Darmstadt, Germany) in compliance with the solution-sample ratio of 20:1.

Tissue processing and paraffin embedding was carried out automatically (Leica TP1020, Leica Biosystems Nussloch GmbH, Nußloch, Germany) in the case of bladder and tunica albuginea patches, while manually for macroscopic sections of prostate and penis according to routine protocols. Thereafter,  $5 \mu\text{m}$  thick sections were cut and stained with Hematoxylin-Eosin (W01030708, BioOptica Milano, Milan, Italy) and Azan-Mallory (04-001802, BioOptica Milano, Milan, Italy) for histological characterization. In both cases, all the sections were deparaffinized with xylene, hydrated through a decreasing scale of alcohol solutions, stained with kit-specific dyes, dehydrated through an increasing scale of alcohol solutions, clarified in xylene and mounted through Eukitt mounting medium (09-00250, BioOptica Milano, Milan, Italy).

#### 2.5. Statistical Analysis

Median, 25th and 75th percentiles were calculated for all the tested samples by using Matlab (MATLAB and Statistics Toolbox Release 2022b, The MathWorks, Inc., Natick, MA, USA). No statistical tests were performed due to the limited number of tests per tissue.

### 3. Results

Mechanical tests were performed to study the different mechanical responses of the tissues composing the LUT, when possible examining the regional and directional tissue variability. From experimental tensile data, the strain was computed as the ratio between the elongation and the initial grip-to-grip length of the specimen, while the stress was computed as the ratio between the force measured by the load cell and the initial cross-sectional area of the sample.

Regarding the failure results, for all tested tissues the stress–strain curves were considered up to the inflection point assumed as the failure point of the tissue. At this point, the stress and strain values were extracted as respectively the ultimate tensile stress (UTS) and the strain at UTS to characterize the mechanical tensile response of the different tissues.

Median curves and confidence intervals for the tissues tested until failure are shown in Figure 2.

The elastic modulus  $E$  was extracted from the linear region of the stress–strain curves, which differs among the tissues. This region corresponded to specific strain ranges according to the tissue: for the bladder [19.42–29.99]%, for the Buck's fascia [13.05, 22.91]%, for the prostate [23.63–19.48]% along the longitudinal direction while [52.51–68.32]% along the transversal one and for the tunica albuginea [9.03, 19.04]% along the longitudinal direction and [10.52–19.02]% along the transversal one.  $E$  was then defined as the slope of these regions, computed by means of linear fitting ( $R^2 > 0.99$ ), as performed in other studies [24,25].

Median values (25th, 75th percentiles) of the UTS, the strain at UTS and the elastic modulus are reported in Table 4. Among all, the highest stiffness of the elastic modulus was exhibited by the tunica albuginea along the transversal direction (median 40.44 MPa, [35.91, 44.97] MPa), followed by its longitudinal direction (12.77 MPa, [10.36, 17.70] MPa), while the lowest one by the prostate along the transversal direction (0.66 MPa, [0.63, 0.86] MPa). In accordance with these results, the tunica albuginea along the transversal

direction showed also the highest UTS, while the minimum strain at UTS was recorded by its longitudinal direction. On the opposite, the prostate along the transversal direction exhibited the greater strain at break. Concerning the anisotropy of the prostate tissue, the elastic modulus, the UTS and the strain at UTS along the longitudinal direction resulted, in median terms, respectively, 2.34, 1.37 and 0.30 times the corresponding values along the transversal direction.

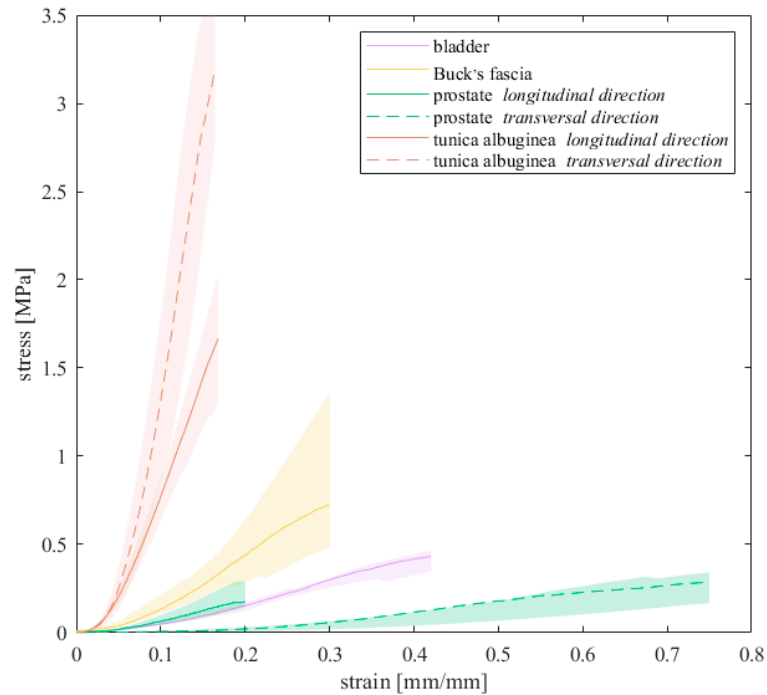


**Figure 2.** Stress–strain curves up to breakage resulted for all the tissues that were subjected to failure tests. Median curves are reported with 50% probability scatter bands.

**Table 4.** For each tissue tensioned up to failure, median values (25th, 75th percentiles) of the elastic modulus, UTS and strain at UTS are reported.

Tissue	E [MPa]	UTS [MPa]	Failure Strain [%]
Bladder	1.40 (1.16, 1.58)	0.47 (0.44, 0.54)	51.42 (47.23, 54.69)
Buck’s fascia	3.86 (2.18, 7.46)	0.86 (0.66, 1.79)	47.79 (42.45, 50.73)
Prostate—L	1.54 (1.13, 2.35)	0.44 (0.26, 0.48)	25.37 (22.62, 45.38)
Prostate—T	0.66 (0.63, 0.86)	0.32 (0.29, 0.41)	85.45 (77.80, 124.19)
Tunica albuginea—L	12.77 (10.36, 17.70)	2.12 (1.39, 3.81)	21.14 (17.91, 26.97)
Tunica albuginea—T	40.44 (35.91, 44.97)	6.50 (3.64, 9.36)	24.27 (16.78, 31.75)

L = longitudinal, T = transversal.

Data from stress–relaxation tests were processed to analyze the response of each tested tissue during and after the relaxation phases. From stress–time data, the relaxation curves were extracted in response to each step strain and, to compare results at the same strain condition, normalized stress data were obtained as the ratio between stresses at the current time and at the beginning of the relaxation phase. Depending on the strain history assumed for each tissue, the normalized stress–time curves were separately determined and fitted by the following exponential formulations:

$$\sigma_{norm}(t) = 1 - \gamma_1 - \gamma_2 + \gamma_1 e^{(-t/\tau_1)} + \gamma_2 e^{(-t/\tau_2)} \tag{1}$$

Equation (1) describes the normalized stress  $\sigma_{norm}$  over time  $t$  and accounts for two viscous branches, whose parameters are  $\gamma_1$  and  $\gamma_2$  as relative stiffness and  $\tau_1$  and  $\tau_2$  as the time constants of relaxation. The number of branches was defined by a trade-off between

the minimization of the number of the parameters and the adequate interpretation of the trend of the experimental data and agrees with previous studies on LUT tissues [8,9]. The quantity  $\gamma_1 + \gamma_2$  accounts for the amount of stress relaxation of the normalized curves (in percentage it represents the degree of relaxation for each tissue). The resulting normalized median stress–time curves and the related 50% probability scatter bands are shown in Figure 3, while fitting parameters are reported in Table 5.

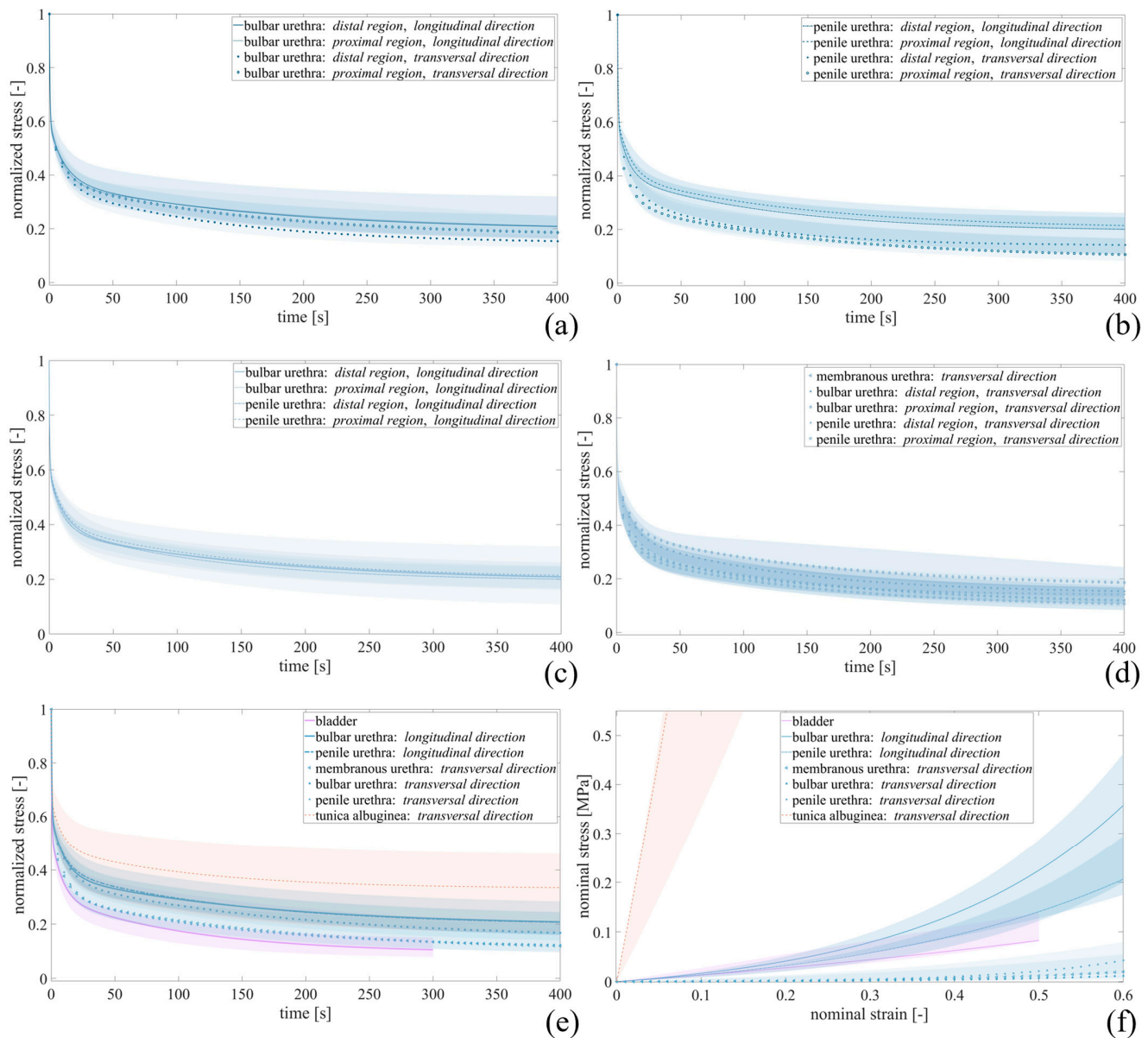


**Figure 3.** Relative stress–relaxation curves resulted for (a) bulbar and (b) penile urethra in distal and proximal regions, for all urethral samples tested along the (c) longitudinal and (d) transversal directions, and for (e) all tissues underwent stress–relaxation test. (f) Stress–strain curves obtained at equilibrium for bladder, tunica albuginea and urethra samples. Median curves are reported together with 50% probability scatter bands.

For the bulbar urethra (Figure 3a), differences in terms of relaxation degree were not found between distal (D) and proximal (P) regions along both the longitudinal (D 78.19%, [74.23, 82.94]%; P 78.12%, [67.24, 82.65]%) and the transversal (D 83.95%, [82.06, 86.26]%; P 80.68%, [76.14, 83.04]%) directions. Similarly, no differences resulted for the penile urethra (Figure 3b) between the D and P regions along the two tested directions.

**Table 5.** From the results of stress–relaxation tests, elastic ( $k$ ,  $\alpha$ ) and viscous ( $\gamma_1$ ,  $\gamma_2$ ,  $\tau_1$ ,  $\tau_2$ ) parameters were obtained in terms of median values.

Tissue	$k$ [kPa]	$\alpha$	$\gamma_1$	$\gamma_2$	$\tau_1$ [s]	$\tau_2$ [s]
Bladder	120	1.20	0.63	0.26	1.01	65.39
Tunica albuginea—T	8640	2.05	0.46	0.20	1.03	68.91
Membranous urethra—T	5.40	4.94	0.63	0.24	1.21	96.26
Bulbar urethra—L	130	4.19	0.56	0.23	1.44	83.10
Bulbar urethra—T	3.00	5.13	0.58	0.25	1.49	104.80
Penile urethra—L	120	3.13	0.55	0.24	1.29	93.84
Penile urethra—T	4.70	6.94	0.60	0.26	1.22	72.56

L = longitudinal, T = transversal.

For these reasons, median values of the resulting parameters  $\gamma_1$ ,  $\gamma_2$ ,  $\tau_1$  and  $\tau_2$  are reported in Table 5 without distinguishing the distal and proximal regions.

Both the bulbar and penile urethral samples suggested different relaxation phases if tested along the longitudinal or the transversal direction. In particular, the penile urethra showed a stress decrease equal to 87.59% [83.31, 90.10]% along the transversal direction, while equal to 79.33% [75.63, 84.03]% along the longitudinal one.

Analyzing all the urethral samples tested longitudinally, the relaxation curves resulted independent of the harvesting region, as shown in Figure 3c. On the other hand, considering all the urethral samples tested transversally (Figure 3d), different urethral regions determined different degrees of relaxation, reporting the maximum value for the penile urethra (87.59%, [83.31, 90.10]%) and the minimum for the bulbar urethra (83.22%, [79.84, 86.02]%). All these curves obtained from urethral samples resulted in an intermediate region between those relating to the tunica albuginea tested along the transversal direction and those related to the bladder (Figure 3e) exhibited a final drop of normalized stress equal to 65.74% [53.47, 82.12]% and 88.55% [84.00, 91.18]%, respectively.

Moreover, original stress–time data were processed to analyze the tissue mechanical response at the end of relaxation phases, when all the time-dependent phenomena completely occurred. By considering the stress at the equilibrium point for each step strain applied for each specimen, non-linear stress ( $\sigma$ )–strain ( $\epsilon$ ) curves were separately obtained and fitted by the following exponential formulation:

$$\sigma(\epsilon) = k/\alpha [e^{(\alpha\epsilon)} - 1] \quad (2)$$

The parameter  $k$  specifies the tissues' initial stiffness, while  $\alpha$  is related to the non-linearity of the response due to the stiffening. For each tissue, the resulting parameters ( $k$ ,  $\alpha$ ) are reported in terms of median in Table 5. It can be observed that, among all the tested tissues, the tunica albuginea exhibited the highest stiffness with a value up to three scale orders above. Stress–strain curves obtained at equilibrium are reported in Figure 3f.

From the indentation test on the prostate sample, the reaction forces and the deformation were acquired for each indentation point.

Under the assumption of the tissue as a semi-infinite elastic body and considering that the indenter perfectly contacted with the tissue,  $E$  was fitted by means of the Hertz-Sneddon equation [13]:

$$F = 4/3 E \left(1 - \nu^2\right)^{-1} \sqrt{R\delta^3} \quad (3)$$

where  $F$  is the maximum value of the reaction force,  $R$  is the indenter radius,  $\delta$  is the indentation depth and  $\nu$  is the Poisson's ratio, assumed equal to 0.499.

Figure 4 shows the mechanical responses resulting from the indentation points P1 and P5, placed in different regions of the prostate sample. In particular, P1 refers to one nodule formation on the prostate, while P5 refers to the non-altered tissue. From the experimental results, only the first part of the curve was fitted, for a maximum indentation depth of 1.5 mm and resulted in a good fit quality (reported in Table 6 by the  $R^2$  parameter).

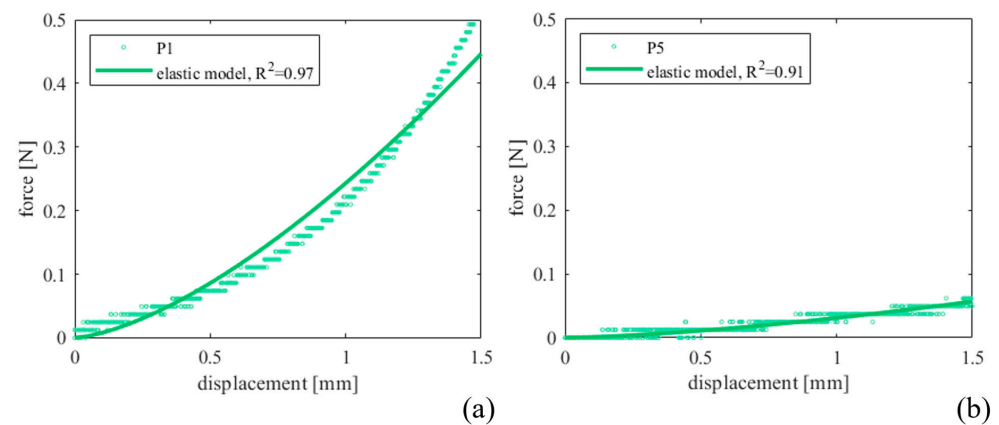


**Figure 4.** Indentation force–depth curves measured for (a) P1 and (b) P5 prostate indentation points and comparison with the fit performed by adopting Equation (3).

**Table 6.** Prostate elastic modulus in MPa (and R<sup>2</sup> in brackets) reported according to the indentation region (P1–P7).

P1	P2	P3	P4	P5	P6	P7
0.077 (0.97)	0.027 (0.98)	0.017 (0.46)	0.015 (0.85)	0.01 (0.91)	0.022 (0.90)	0.034 (0.98)

With reference to the histological analyses, Hematoxylin–Eosin staining was performed to observe the general layout of the tissues, as reported in Figure 5a,c for the prostate and bladder, respectively, and Figure 6 for the urethra, Buck’s fascia and tunica albuginea. This specific staining highlights the prostate tubuloacinar glands surrounded by fibromuscular stroma (Figure 5a). Furthermore, Figure 6a shows both the urethral section as well as the corpora cavernosa. At the lower center (Figure 6b), the corpus spongiosum surrounding the bulbar urethra is clearly visible.

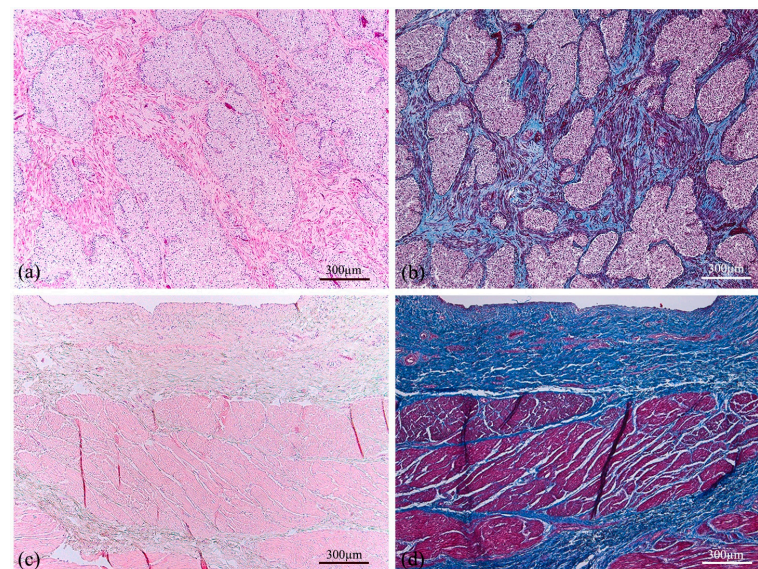


**Figure 5.** Cross section of human prostate (a,b) showing tubuloacinar glands surrounded by fibromuscular stroma. Transversal section of the human bladder (c,d) presenting the mucosa, submucosa, and first muscle layers. Both tissue sections were stained with Haematoxylin–Eosin (a,c) and Azan–Mallory (b,d).

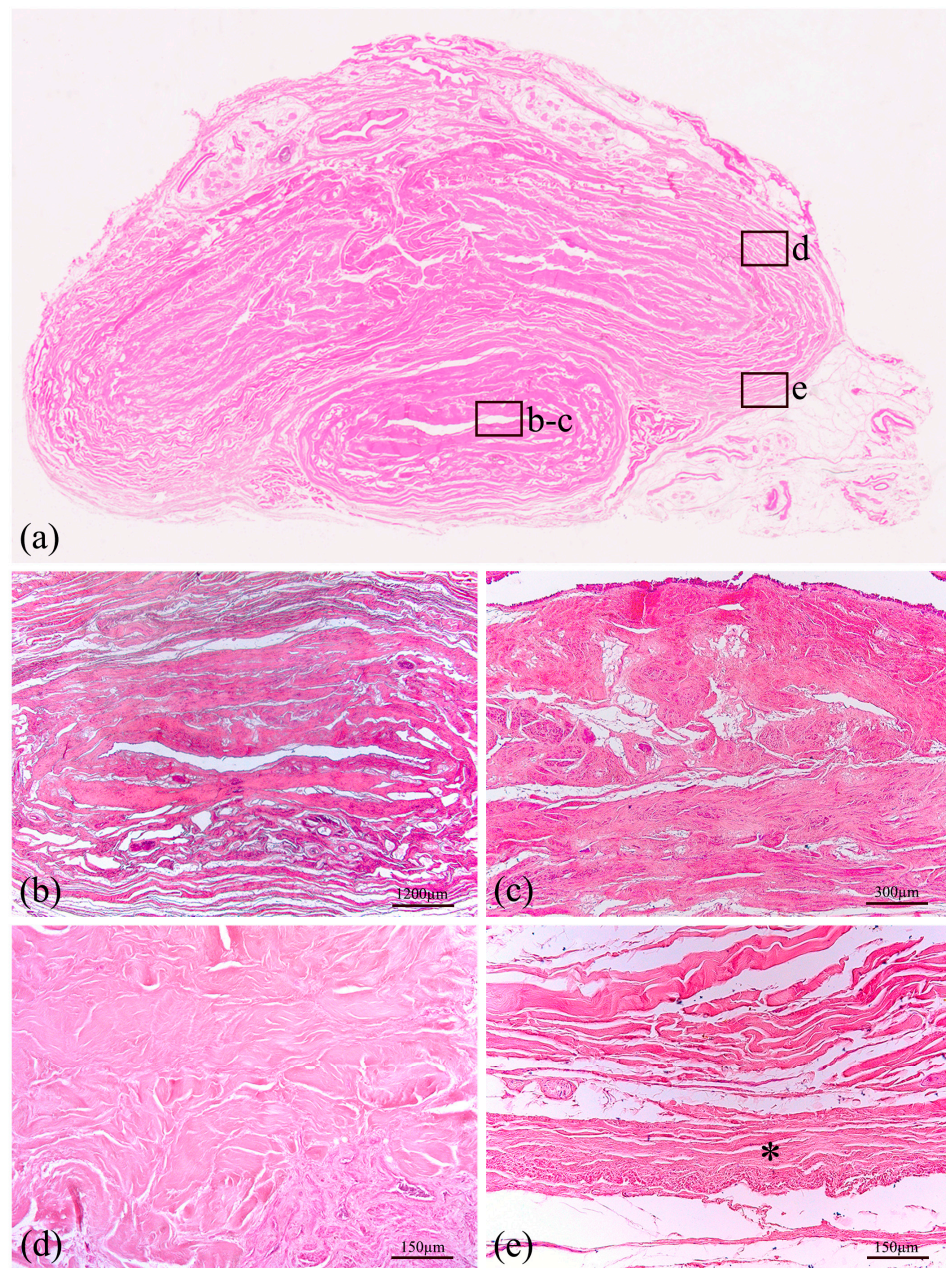


**Figure 6.** Histological representation of large thickness specimen of the human penis (a) stained with Haematoxylin–Eosin. The section at the lower center is the corpus spongiosum surrounding the bulbar urethra, shown at two different magnifications (b,c). In the upper part of the macrosection, two corpora cavernosa are surrounded by tunica albuginea (d). All these structures are covered by Buck’s fascia, a deep fascia layer made of fibrous connective tissue, indicated by an asterisk (e).

Additional staining (Azan–Mallory) was performed to distinguish muscle fiber content with red color and connective tissue, highlighting collagen fibers with blue color (Figures 5b,d and 7). Therefore, the tunica albuginea (Figure 7d) around the corpora cavernosa can be noticed, as well as the Buck’s fascia (Figure 7e), which results in a deep fascia layer made of fibrous connective tissue, indicated by an asterisk. Moreover, the transversal section of the human bladder (Figure 5d) reveals the mucosa, submucosa and first muscle layers.

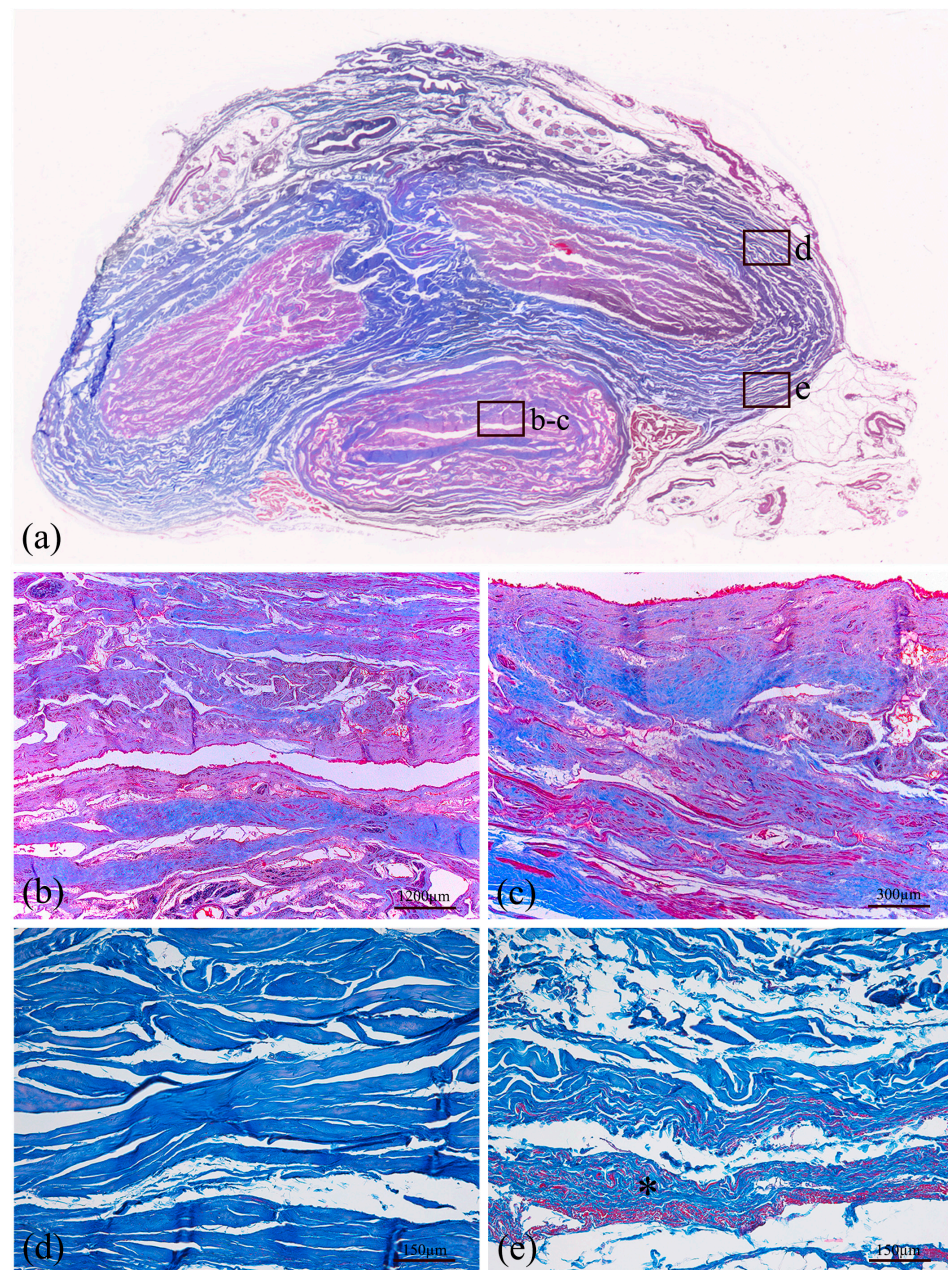


**Figure 7.** Histological representation of a transversal section of the human penis (a) stained with Azan–Mallory. The section at the lower center is the bulbar urethra surrounded by corpus spongiosum and shown at two different magnifications (b,c). In the upper part of the macrosection, two corpora cavernosa are surrounded by tunica albuginea (d). All these structures are covered by Buck’s fascia, a deep fascia layer made of fibrous connective tissue, indicated by an asterisk (e).

#### 4. Discussion

Human LUT biomechanics research is in its infancy, different from research on many human tissues that have already extensively investigated. On the basis of the literature, currently, few works have been published on the mechanical investigation of some of these biological tissues, while others have never been studied before or only partially.

Moreover, biological tissues are usually characterized by a huge inter-subject variability due to a variety of factors such as subject age, gender, BMI and similar. This usually affects the results when the focus is the quantification of the difference between tissues from the same anatomical district. For this reason, the present study reported the mechanical characterization of the tissues of the LUT harvested from the same subject and tested with

the same protocols to quantify each tissue's contribution to the overall mechanical response of the district.

Figure 2 reports the median failure curves that were obtained for the bladder, the Buck's fascia, the prostate and the tunica albuginea, with mechanical characteristics listed in Table 4. As a first analysis, the bladder and prostate exhibited similar tensile behavior in terms of UTS and  $E$  of the linear region, while strain at break spans for all the tissues from about 21% up to 85%. Tunica albuginea resulted in the stiffest tissue, with a UTS of about four times greater than the others, with  $E$  increasing by one order of magnitude. The bladder showed a restrained variability, suggesting no predominant fibers distribution, while clear differences were observed for the prostate and the tunica, even if, for the latter, the number of samples was limited.

Animal bladder tissues were analyzed by Zanetti et al. [9], who studied the effect of strain rate, orientation and loading history on the behavior in porcine, and then added uniaxial cyclic tests at different strain rates (10, 50, 100, 200, 500%  $s^{-1}$ ) reaching a strain of about 50% [10]. Contrary to what has been observed in this study, porcine bladders showed greater stiffness along the transverse loading direction and were more influenced by the strain rate than those tested along the apex-to-base ones, even if they observed a homogeneous distribution of collagen fibers in the animal tissue. In the present work, the human bladder strain reached in the loading phase was lower (51.42%, [47.23, 54.69]%) than the strain values reported for porcine, whose loading phase covered a final strain of 100% adopting similar strain rates (1.3%  $s^{-1}$  in [9] while 2.5%  $s^{-1}$  in this protocol), but with higher recorded stresses (0.47 MPa, [0.44, 0.54] MPa vs about 0.05 MPa [9]). On the basis of the thickness measurements, the pig bladder samples resulted as thicker than the human ones in the present work ( $3.99 \pm 1.04$  mm [9] and  $4.37 \pm 1.00$  mm [10] vs.  $2.14 \pm 0.31$  mm).

Our results in human samples are also supported by the histological analysis as well as motivated by their physiological function. In particular, histological staining with Haematoxylin–Eosin (Figure 6) and Azan–Mallory (Figure 7) was performed to identify the gross appearance and more specific tissue composition of human specimens. Figure 7 shows the muscle (red) and connective tissue (blue) distribution, distinguishing between compact tissue near the urethral lumen and porous tissue on the outer side, represented by corpus spongiosum. Concerning urethral tissue, the second magnification in Figure 7b shows the different layers of the urethra transversal section, indicating the main layers and fiber directions. The two different muscle fiber directions confirm the mechanical behavior of the tissue, supporting also the data of Cunnane et al., 2021 [5] and Masri et al., 2018 [4].

To investigate the prostatic fibrosis as responsible for LUT dysfunctions, Ma et al. [15] collected an entire prostate from a cadaver (66 years) and periurethral tissue from 28 men undergoing radical prostatectomy. Similar to the here reported protocol, the prostate was opened along the urethra and slices were taken parallel and perpendicular to the urethra (thickness  $3.3 \pm 0.4$  mm), while prostatectomy tissues were trimmed in strips, whose thickness ( $2.0 \pm 0.6$  mm) resulted very similar to the measures of the present study ( $1.96 \pm 0.62$  mm). When considering the healthy tissue, they found an average tangent modulus of  $450 \pm 77$  kPa for the samples parallel to the urethra while  $560 \pm 180$  kPa for the perpendicular samples, reporting a minor difference between the two directions if compared to the results of the present study, even if adopting similar strain rate (1%  $s^{-1}$  up to a maximum strain of 30%), as well as lower absolute values. In the meantime, the prostatectomy tissues reported a wider range of tangent modulus between 9 and 2390 kPa with greater stiffness directly correlated with higher collagen content due to fibrosis and with moderate/severe LUT symptoms. These results could support the evidence of a reparative adaptation of the prostate tissue in response to the endoscopic intervention documented in the donor's health history (TURP), which was characterized by a stiffer response along both directions (Table 4), but maintaining the anisotropic behavior due to a non-homogeneous fibers distribution (Figure 5).

The human tunica albuginea was only partially studied in healthy conditions with unique methods [16], but because of the particular testing technique, it was difficult to

compare the results to those obtained in the present study. However, the thickness values were very similar ( $2.42 \pm 0.53$  mm [16] vs.  $2.38 \pm 0.52$  mm). Regarding the mechanical basis of pathological conditions, Brady et al. [17] proposed uniaxial tensile tests up to failure (strain rate  $1 \text{ mm s}^{-1}$ ) of the tunica albuginea affected by PD. Specimens exhibited high variability in mechanical properties ( $E$  of 5–118 MPa, UTS 1.1–6.1 MPa and strain at UTS 9–42%). These findings showed an altered tissue behavior with mineralization, supported by the literature studies on atherosclerotic plaque mechanics which found higher modulus [19–21] in calcified plaques compared to healthy tissue. Healthy tunica albuginea samples tested in the present study showed mechanical properties close to the lower limit of the wide range shown in [17]. Tensile strength and Young's modulus of tunica albuginea were also evaluated in a primate model by Kandabarow et al. [18], reporting, respectively, an average value of  $1.9 \pm 0.4$  MPa and  $11.9 \pm 4.2$  MPa along the circumferential direction, very close to the values obtained longitudinally in the present study (UTS 2.12 MPa, [1.39, 3.81] MPa;  $E$  12.77 MPa, [10.36, 17.70] MPa).

Referring to the viscoelastic behavior of the human LUT tissues, stress–relaxation tests were performed in this work. Figure 3a–d report the normalized relaxation curves of the urethra when considering different regions (membranous, penile or bulbar), locations (distal or proximal) and directions (longitudinal or transverse). No significant differences were observed varying the regions or the location, with similar percentages of relaxation between about 78% and 88%. The only exception can be seen when comparing the loading direction within the penile region, where a difference of about 10% of relaxation between the longitudinal and the transverse directions was observed. Narrowed confidence intervals showed a good repeatability of the relaxation phenomenon among the samples. Figure 3e showed the comparison with other tissues, i.e., the bladder and the tunica albuginea (only transversal direction was reported due to sample availability). The tunica albuginea had the lowest percentage of relaxation (65.74%, [53.47, 82.12]%), while bladder behavior appeared similar to those of the urethral tissues (88.55%, [84.00, 91.18]%).

Clear anisotropy can be observed between longitudinal and transversal urethral samples when referring to the stress–strain equilibrium curves (Figure 3f). The human urethra exhibited a stiffer response along its axis, while circumferential deformations can be achieved with lower stresses. These insights are also supported by the functional evidence during micturition, where the urine flow applies a radial pressure thus resulting in a predominant radial urethral deformation rather than a longitudinal one. Table 5 reports all the fitting parameters of the different tissues, underlining that, for the equilibrium, the initial stiffness  $k$  for the transversal urethral direction is two orders of magnitude lower than the longitudinal one. As during failure, in the equilibrium response, tunica albuginea was the tissue characterized by the greatest initial stiffness (8.64 MPa).

Few other works reported the viscoelastic characterization of human LUT tissues. Masri et al. [4] found that the spongy urethra exhibited more important hysteresis and anisotropy, with a stiffer behavior in the circumferential direction. Contrary to our findings, Cunnane et al. [5] reported no differences between regional responses for circumferential or longitudinal extension and also in terms of the relaxation or creep parameters defining the response in the two directions, while Natali et al. [8] reported greater stiffness for the proximal specimens of equine urethra along the longitudinal direction, as in the present study. A significant difference in terms of stiffness resulted when comparing the longitudinal proximal specimens to all the other samples. Comparing thickness measurements of human urethral strips, the mean value recorded in the present study ( $3.73 \pm 0.78$  mm) is within the range outlined by the literature studies mentioned above ( $2.53 \pm 0.24$  mm [4],  $4.44 \pm 0.64$  mm [5]).

Stress–relaxation results on porcine bladder samples reported by Zanetti et al. [9] highlighted a longer relaxation time for animal samples ( $>600$  s) with respect to human samples (after 300 s the relaxation phenomenon lasted). In agreement with the present study, they found no differences among the loading directions in terms of viscosity. Even in humans, the regular spatial distribution of the contractile and support elements has

been observed in the various layers of the bladder wall (Figure 5). The bladder can be seen as a three-dimensional multiplanar interweaving structure that allows the forces to be uniformly distributed both in expansion and contraction. This conformation ensures a gradual and coordinated modification of bladder diameters during physiological activity, with greater involvement of the dome and lateral walls.

Finally, to investigate LUT biomechanics under additional loading combinations, the compression behavior of the prostate was also analyzed through indentation tests. Figure 4 shows the recorded force between 0 and 1.5 mm of indentation depth and the curves obtained by fitting the experimental data with the elastic Hertz model (Table 6,  $R^2 > 0.85$  for all the points with only P3 as an exception). Since the prostate reported some signs of TURP with portions of the gland tissue covered by nodules, points P1, P2 and P7 investigated the stiffness of the nodule surface, then compared with the other points. On average, nodule elastic modulus resulted in  $46 \pm 27$  kPa, three times greater with respect to the other regions without repair signs ( $16 \pm 5$  kPa). This is consistent with what is known about the repair processes of damaged tissues by surgical procedures, such as endoscopic resection for the clinical diagnosis of benign prostatic hyperplasia in the present case. As expected, the proliferation of connective tissue with a share of elastic fibers consequently leads to different behavior of the repaired tissue compared to the native one. Other studies in the literature reported indentation on prostate glands, especially in pathological conditions. In particular, our outcomes resulted in good agreement with Ahn et al. [13], who performed indentation tests on prostate specimens from 46 patients undergoing radical prostatectomy by adopting a minimally motorized indenter with a hemisphere tip and cylindrical probe (diameter 2 mm) and a similar protocol (3 mm depth indentation at a speed of  $1 \text{ mm s}^{-1}$ ). The Hertz–Sneddon equation was also applied to estimate the elastic modulus with Poisson’s ratio of 0.499. The results showed that the region containing cancerous tissue increased the elastic modulus ( $24.1 \pm 14.5$  kPa vs.  $17.0 \pm 9.0$  kPa). In addition, Kim et al. [14] investigated the relationship between prostate elasticity and LUT dysfunctions. According to indentation results on 48 prostates from patients (age  $65.8 \pm 5.9$  years) who underwent radical prostatectomy, the median elastic modulus was 20.8 kPa [5.6–22.9] kPa, and the incidences of the LUT dysfunctions were significantly higher in patients with an elastic modulus  $> 20$  kPa.

As this work is the first comprehensive analysis of LUT biomechanics able to exclude possible bias due to inter-subject variability, there are some limitations that should be mentioned. First of all, the number of samples obtained for each tissue in some cases was scarce and thus no statistical analysis was provided as additional support to these findings. However, even if one single case study could result in limited sample availability, narrowed confidence intervals could confirm the advantage of comparing tissues from the same source. Indeed, within this study, attention was primarily paid to underlining the difference between tissues mechanical behavior, functions and composition, and it is possible to conclude that the results clearly highlighted differences and similarities (Figures 2 and 3).

Differences among the experimental setup could have affected some comparisons. Rings vs rectangular samples for tensile tests on the urethra were prepared differently (i.e., for the second group, a sample holder was provided and the samples were attached by means of strong rapid glue). However, no specific sample damage or alteration was observed at the end of the test for either setup, suggesting suitable results for both procedures.

Sample storage could be seen as another limitation. However, after sample harvesting from the cadaver ( $-80$  °C), all the patches were kept at  $-20$  °C, a temperature that was reported to not significantly influence LUT tissues’ mechanical performances [7]. Moreover, all the tests were performed in a limited interval of time; thus, samples were stored at this temperature for no more than two months. Comparison with the literature confirmed the reliability of the obtained results.

## 5. Conclusions

The contribution of the work here proposed is two-fold and it is suitable to fill a clearly missing piece in the literature: for the first time, mechanical tests were carried out on human Buck's fascia, and all the LUT tissues for the mechanical investigation were harvested from the same subject with the potential to highlight the characteristic behavior of the different tissues avoiding the variability due to tissues from different patients.

Currently, this case study sets the basis for the investigation approach for future developments which would require the extension of the numerosity of the population samples to improve the experimental data reliability. Characterization of the essential mechanical properties of the LUT may represent a key aspect for the development of effective *in silico* models to extend the experimental results to high-level scenarios providing additional information on LUT dysfunctions and reliable diagnostic and/or therapeutic tools for the urological clinical and surgical context [26–28]. The study and validation process of innovative procedures and devices for the treatment of LUT pathologies, such as balloon catheters for dilating urethral strictures or artificial sphincters for restoring urinary continence condition [29–33], needs to be considered according to the mechanical behavior of the biological tissues and structures involved, as well as the development and suitability of phantoms mimicking the tissue performance for surgical planning and training [34] and the tissue engineering for surgical reconstruction of anatomical or functional defects [35,36].

**Author Contributions:** Conceptualization, A.B., R.B.-B. and E.L.C.; methodology, A.B., M.V.M., C.G.F. and R.B.-B.; software, A.B. and M.V.M.; validation, A.B., M.V.M., C.G.F. and R.B.-B.; formal analysis, M.V.M.; investigation, A.B., M.V.M., M.C. and M.T.; resources, A.P., V.M., R.D.C. and E.L.C.; data curation, A.B., M.V.M. and R.B.-B.; writing—original draft preparation, A.B. and M.V.M.; writing—review and editing, A.B., M.V.M., C.G.F., M.C., M.T., R.B.-B. and E.L.C.; supervision, A.B., C.G.F., R.B.-B. and E.L.C.; project administration, A.P., V.M. and E.L.C.; funding acquisition, C.G.F. and E.L.C. All authors have read and agreed to the published version of the manuscript.

**Funding:** This work was supported by MIUR, FISR 2019, Project no. FISR2019\_03221, titled CE-COMES: CEntro di studi sperimentali e COmputazionali per la ModElliStica applicata alla chirurgia and by University of Padova, Project FONT\_BIRD2020\_01, titled Characterization of Artificial Urinary Sphincters for the identification of new DEVices (AUS-DEV).

**Institutional Review Board Statement:** All procedures were conducted on human bodies from the “Donation to Science” Body Donation Program of the University of Padova and Veneto Region/National Reference Center for preserving and using gifted bodies. The procedures were carried out in accordance with national laws, ethical standards of the regional/national research committees, and the 1964 Helsinki Declaration, including its later amendments or comparable ethical standards. Participants provided written informed consent to join the Body Donation Program, which has met the requirements of standard ISO 9001:2015 (Registration number: IT-62435-16764) (ISO, 2008). The privacy rights of human subjects were and will always be respected.

**Informed Consent Statement:** Informed consent was obtained from all subjects involved in the study, consistently with the setting of collection/donation of the anatomical material.

**Data Availability Statement:** The raw/processed data are available, contacting the corresponding authors, on reasonable request. The article contains all the necessary health data of the body donors, which can/should be utilized for scientific research purposes based on the informed consent provided. Any additional information that is not relevant or useful to the research is kept private and not disclosed to protect the privacy of the individuals.

**Conflicts of Interest:** The authors declare no conflicts of interest.

## References

1. Mahadevan, V. Anatomy of the lower urinary tract. *Surgery* **2016**, *34*, 318–325. [[CrossRef](#)]
2. Dunnick, N.R.; Sandler, C.M.; Jeffrey, H. *Newhouse, Textbook of Uroradiology*, 5th ed.; Lippincott Williams & Wilkins: Philadelphia, PA, USA, 2012.
3. Singh, G.; Chanda, A. Mechanical properties of whole-body soft human tissues: A review. *Biomed. Mater.* **2021**, *16*, 062004. [[CrossRef](#)] [[PubMed](#)]

4. Masri, C.; Chagnon, G.; Favier, D.; Sartelet, H.; Girard, E. Experimental characterization and constitutive modeling of the biomechanical behavior of male human urethral tissues validated by histological observations. *Biomech. Model. Mechanobiol.* **2018**, *17*, 939–950. [[CrossRef](#)] [[PubMed](#)]
5. Cunnane, E.M.; Davis, N.F.; Cunnane, C.V.; Lorentz, K.L.; Ryan, A.J.; Hess, J.; Weinbaum, J.S.; Walsh, M.T.; O'Brien, F.J.; Vorp, D.A. Mechanical, compositional and morphological characterisation of the human male urethra for the development of a biomimetic tissue engineered urethral scaffold. *Biomaterials* **2021**, *269*, 120651. [[CrossRef](#)] [[PubMed](#)]
6. Lalla, M.; Danielsen, C.C.; Austevoll, H.; Olsen, L.H.; Jørgensen, T.M. Biomechanical and Biochemical Assessment of Properties of the Anterior Urethra After Hypospadias Repair in a Rabbit Model. *J. Urol.* **2007**, *177*, 2375–2380. [[CrossRef](#)] [[PubMed](#)]
7. Cunnane, C.V.; Croghan, S.M.; Walsh, M.T.; Cunnane, E.M.; Davis, N.F.; Flood, H.D.; Mulvihill, J.J. Cryopreservation of porcine urethral tissue: Storage at  $-20^{\circ}\text{C}$  preserves the mechanical, failure and geometrical properties. *J. Mech. Behav. Biomed. Mater.* **2021**, *119*, 104516. [[CrossRef](#)]
8. Natali, A.N.; Carniel, E.L.; Frigo, A.; Pavan, P.G.; Todros, S.; Pachera, P.; Fontanella, C.G.; Rubini, A.; Cavicchioli, L.; Avital, Y.; et al. Experimental investigation of the biomechanics of urethral tissues and structures. *Exp. Physiol.* **2016**, *101*, 641–656. [[CrossRef](#)]
9. Zanetti, E.M.; Perrini, M.; Bignardi, C.; Audenino, A.L. Bladder tissue passive response to monotonic and cyclic loading. *Biorheology* **2012**, *49*, 49–63. [[CrossRef](#)]
10. Natali, A.N.; Audenino, A.L.; Artibani, W.; Fontanella, C.G.; Carniel, E.L.; Zanetti, E.M. Bladder tissue biomechanical behavior: Experimental tests and constitutive formulation. *J. Biomech.* **2015**, *48*, 3088–3096. [[CrossRef](#)]
11. Krouskop, T.A.; Wheeler, T.M.; Kallel, F.; Garra, B.S.; Hall, T. Elastic Moduli of Breast and Prostate Tissues Under Compression. *Ultrason. Imaging* **1998**, *20*, 260–274. [[CrossRef](#)]
12. Phipps, S.; Yang, T.H.J.; Habib, F.K.; Reuben, R.L.; McNeill, S.A. Measurement of the mechanical characteristics of benign prostatic tissue: A Novel method for assessing benign prostatic disease. *Urology* **2005**, *65*, 1024–1028. [[CrossRef](#)] [[PubMed](#)]
13. Ahn, B.M.; Kim, J.; Ian, L.; Rha, K.H.; Kim, H.J. Mechanical property characterization of prostate cancer using a minimally motorized indenter in an ex vivo indentation experiment. *Urology* **2010**, *76*, 1007–1011. [[CrossRef](#)]
14. Kim, K.H.; Ahn, B.; Lim, S.K.; Han, W.K.; Kim, J.H.; Rha, K.H.; Kim, J. Indenter study: Associations between prostate elasticity and lower urinary tract symptoms. *Urology* **2014**, *83*, 544–549. [[CrossRef](#)]
15. Ma, J.; Gharaee-Kermani, M.; Kunju, L.; Hollingsworth, J.M.; Adler, J.; Arruda, E.M.; Macoska, J.A. Prostatic fibrosis is associated with lower urinary tract symptoms. *J. Urol.* **2012**, *188*, 1375–1381. [[CrossRef](#)]
16. Bitsch, M.; Kromann-Andersen, B.; Schou, J.; Sjøntoft, E. The Elasticity and the Tensile Strength of Tunica Albuginea of the Corpora Cavernosa. *J. Urol.* **1990**, *143*, 642–645. [[CrossRef](#)] [[PubMed](#)]
17. Brady, L.; Stender, C.J.; Wang, Y.-N.; Schade, G.R.; Maxwell, A.D.; Wessells, H.; Ledoux, W.R. Mechanical characterization of fibrotic and mineralized tissue in Peyronie's disease. *Int. J. Impot. Res.* **2022**, *34*, 477–486. [[CrossRef](#)]
18. Kandabarow, A.M.; Chuang, E.; McKenna, K.; Le, B.; McVary, K.; Colombo, A. Tensile strength of penile tunica albuginea in a primate model. *J. Urol.* **2021**, *206*, 1073. [[CrossRef](#)]
19. Sherebrin, M.H.; Bernans, H.A.; Roach, M.R. Extensibility Changes of Calcified Soft Tissue Strips from Human Aorta. *Can. J. Physiol. Pharmacol.* **1987**, *65*, 1878–1883. [[CrossRef](#)]
20. Walraevens, J.; Willaert, B.; De Win, G.; Ranftl, A.; De Schutter, J.; Sloten, J.V. Correlation between compression, tensile and tearing tests on healthy and calcified aortic tissues. *Med. Eng. Phys.* **2008**, *30*, 1098–1104. [[CrossRef](#)]
21. Loree, H.M.; Grodzinsky, A.J.; Park, S.Y.; Gibson, L.J.; Lee, R.T. Static circumferential tangential modulus of human atherosclerotic tissue. *J. Biomech.* **1994**, *27*, 195–204. [[CrossRef](#)]
22. Porzionato, A.; Macchi, V.; Stecco, C.; Mazzi, A.; Rambaldo, A.; Sarasin, G.; Parenti, A.; Scipioni, A.; De Caro, R. Quality management of Body Donation Program at the University of Padova. *Anat. Sci. Educ.* **2012**, *5*, 264–272. [[CrossRef](#)]
23. Biomomentum Catalog. Available online: <https://www.biomomentum.com/catalog/> (accessed on 1 September 2023).
24. Bonaldi, L.; Berardo, A.; Pirri, C.; Stecco, C.; Carniel, E.L.; Fontanella, C.G. Mechanical Characterization of Human Fascia Lata: Uniaxial Tensile Tests from Fresh-Frozen Cadaver Samples and Constitutive Modelling. *Bioengineering* **2023**, *10*, 226. [[CrossRef](#)]
25. Zwirner, J.; Babian, C.; Ondruschka, B.; Schleifenbaum, S.; Scholze, M.; Waddell, N.J.; Hammer, N. Tensile properties of the human iliotibial tract depend on height and weight. *Med. Eng. Phys.* **2019**, *69*, 85–91. [[CrossRef](#)]
26. Mascolini, M.V.; Fontanella, C.G.; Berardo, A.; Carniel, E.L. Influence of transurethral catheters on urine pressure-flow relationships in males: A computational fluid-dynamics study. *Comput. Methods Programs Biomed.* **2023**, *238*, 107594. [[CrossRef](#)]
27. Herwig, R.; Bayerl, M. Superficial tunica albuginea rupture as initial starting point of Peyronie's disease: A topic for interdisciplinary consideration. *Biomed. Res. Int.* **2015**, *2015*, 751372. [[CrossRef](#)] [[PubMed](#)]
28. Wang, F.; Cao, Z.; Zhai, L.; Zhang, J.; Kong, H.; Lin, W.; Fan, Y. Biomechanical study of the male lower urinary tract: Simulation of internal and external sphincters dyssynergia. *J. Biomech.* **2023**, *149*, 111475. [[CrossRef](#)] [[PubMed](#)]
29. Toniolo, I.; Mascolini, M.V.; Carniel, E.L.; Fontanella, C.G. Artificial sphincters: An overview from existing devices to novel technologies. *Artif. Organs* **2022**, *47*, 617–639. [[CrossRef](#)] [[PubMed](#)]
30. Natali, A.N.; Fontanella, C.G.; Carniel, E.L. Biomechanical analysis of the interaction phenomena between artificial urinary sphincter and urethral duct. *Int. J. Numer. Method. Biomed. Eng.* **2020**, *36*, e3308. [[CrossRef](#)] [[PubMed](#)]

31. Mascolini, M.V.; Fogang, J.V.F.; Salomoni, V.; Fontanella, C.G.; Carniel, E.L.; Natali, A.N. A novel artificial urinary sphincter and comparison with reference device. In Proceedings of the 8th National Congress of Bioengineering, GNB 2023, Padova, Italy, 21–23 June 2023; Patron Editore S.r.l.: Bologna, Italy, 2023.
32. Bhave, A.; Sittkus, B.; Urban, G.; Mescheder, U.; Möller, K. Finite element analysis of the interaction between high-compliant balloon catheters and non-cylindrical vessel structures: Towards tactile sensing balloon catheters. *Biomech. Model. Mechanobiol.* **2023**, *22*, 2033–2061. [[CrossRef](#)] [[PubMed](#)]
33. De Menech, Q.; Konstantinidi, S.; Martinez, T.; Benouhiba, A.; Civet, Y.; Perriard, Y. Mechanical Characterisation of Porcine Urethra: Non Linear Constitutive Models and Experimental Approach. In Proceedings of the International Conference on Advances in Biomedical Engineering, Dubai, UAE, 16–17 December 2023; ICABME, Institute of Electrical and Electronics Engineers Inc.: New York, NY, USA, 2023; pp. 35–40. [[CrossRef](#)]
34. Verstraeten, M.; Kheir, G.B.; Perre, L.V.; Raffoul, R.; Cerda, J.C.; Delchambre, A.; Roumeguere, T.; Vanhoestenbergh, A.; Nonclercq, A. Urinary bladder phantom mimicking mechanical properties and pressure during filling. *Biomed. Phys. Eng. Express* **2023**, *9*, 055006. [[CrossRef](#)] [[PubMed](#)]
35. Sartoneva, R.; Lyyra, I.; Juusela, M.; Sharma, V.; Huhtala, H.; Massera, J.; Kellomäki, M.; Miettinen, S. In vitro biocompatibility of polylactide and polybutylene succinate blends for urethral tissue engineering. *J. Biomed. Mater. Res. B Appl. Biomater.* **2023**, *111*, 1728–1740. [[CrossRef](#)] [[PubMed](#)]
36. Cheng, Q.; Zhang, L.; Zhang, J.; Zhou, X.; Wu, B.; Wang, D.; Wei, T.; Shafiq, M.; Li, S.; Zhi, D.; et al. Decellularized Scaffolds with Double-Layer Aligned Microchannels Induce the Oriented Growth of Bladder Smooth Muscle Cells: Toward Urethral and Ureteral Reconstruction. *Adv. Healthc. Mater.* **2023**, *12*, e2300544. [[CrossRef](#)] [[PubMed](#)]

**Disclaimer/Publisher’s Note:** The statements, opinions and data contained in all publications are solely those of the individual author(s) and contributor(s) and not of MDPI and/or the editor(s). MDPI and/or the editor(s) disclaim responsibility for any injury to people or property resulting from any ideas, methods, instructions or products referred to in the content.